Attention Guided Anomaly Localization in Images

Shashanka Venkataramanan$^{\star[0000-0003-1096-1342]}$, Kuan-Chuan
Peng$^{\dagger[0000-0002-2682-9912]}$, Rajat Vikram Singh$^{\ddagger[0000-0002-1416-8344]}$, and
Abhijit Mahalanobis$^{\star[0000-0002-2782-8655]}$

*Center for Research in Computer Vision, University of Central Florida, Orlando, FL
†Mitsubishi Electric Research Laboratories, Cambridge, MA
‡Siemens Corporate Technology, Princeton, NJ
shashankv@Knights.ucf.edu, kpeng@merl.com, singh.rajat@siemens.com,
amahalan@crcv.ucf.edu

Abstract. Anomaly localization is an important problem in computer
vision which involves localizing anomalous regions within images with
applications in industrial inspection, surveillance, and medical imaging.
This task is challenging due to the small sample size and pixel coverage of
the anomaly in real-world scenarios. Most prior works need to use anoma-
lous training images to compute a class-specific threshold to localize
anomalies. Without the need of anomalous training images, we propose
Convolutional Adversarial Variational autoencoder with Guided Atten-
tion (CAVGA), which localizes the anomaly with a *convolutional latent
variable* to preserve the spatial information. In the unsupervised setting,
we propose an *attention expansion loss* where we encourage CAVGA to
focus on all normal regions in the image. Furthermore, in the weakly-
supervised setting we propose a *complementary guided attention loss*,
where we encourage the attention map to focus on all normal regions
while minimizing the attention map corresponding to anomalous regions
in the image. CAVGA outperforms the state-of-the-art (SOTA) anomaly
localization methods on MVTec Anomaly Detection (MVTAD), modified
ShanghaiTech Campus (mSTC) and Large-scale Attention based Glau-
coma (LAG) datasets in the unsupervised setting and when using only
2% anomalous images in the weakly-supervised setting. CAVGA also out-
performs SOTA anomaly detection methods on the MNIST, CIFAR-10,
Fashion-MNIST, MVTAD, mSTC and LAG datasets.

Keywords: guided attention, anomaly localization, convolutional ad-
versarial variational autoencoder

1 Introduction

Recognizing whether an image is homogeneous with its previously observed dis-
tribution or whether it belongs to a novel or anomalous distribution has been
identified as an important problem [5]. In this work, we focus on a related task,
anomaly localization in images, which involves segmenting the anomalous regions

arXiv:1911.08616v4 [cs.CV] 17 Jul 2020

dataset	task	improvement
MVTAD [5]	l	(9/15; 4∼85%)
MVTAD [5]	d	(9/15; 2∼30%)
mSTC [31]	l	(7/12; 2∼42%)
mSTC [31]	d	(8/12; 1∼38%)
LAG [29]	l	(1/1; 16%)
LAG [29]	d	(1/1; 1.1%)
MNIST [27]	d	(8/10; 0.1∼2.5%)
CIFAR-10 [25]	d	(7/10; 3∼31%)
F-MNIST [57]	d	(8/10; 2∼24%)

l: localization; d: detection
F-MNIST: Fashion-MNIST [57]

- metric for l : IoU
- metric for d in MVTAD, mSTC, and LAG: classification accuracy
- metric for d in MNIST, CIFAR-10 and Fashion-MNIST: area under ROC curve

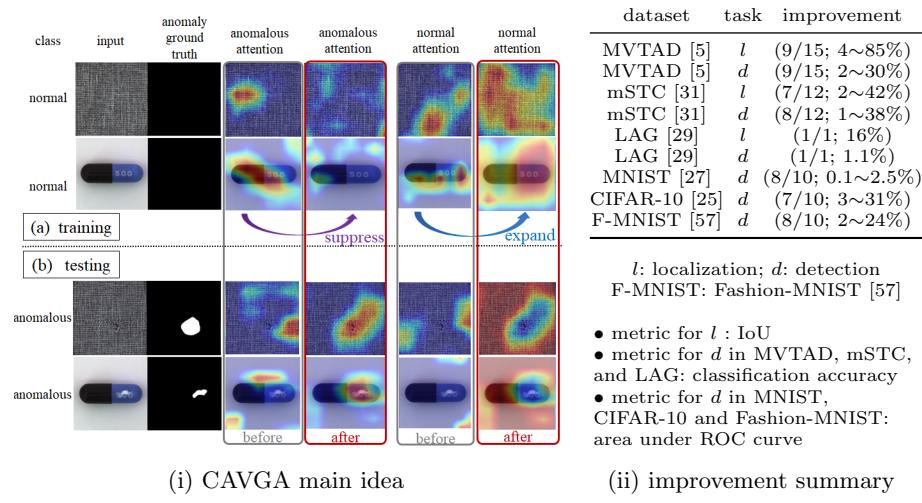(i) CAVGA main idea   (ii) improvement summary

Fig. 1: (i) CAVGA uses the proposed complementary guided attention loss to encourage the attention map to cover the entire normal regions while suppressing the attention map corresponding to anomalous class in the training image. This enables the trained network to generate the anomalous attention map to localize the anomaly better at testing (ii) CAVGA's improvement over SOTA in the form of (number of outperforming/total categories; improvement (%) in its metric)

within them. Anomaly localization has been applied in industrial inspection settings to segment defective product parts [5], in surveillance to locate intruders [38], in medical imaging to segment tumor in brain MRI or glaucoma in retina images [4, 29], etc. There has been an increase in analysis towards segmenting potential anomalous regions in images as acknowledged in [13].

Existing state-of-the-art (SOTA) anomaly localization methods [6, 47] are based on deep learning. However, developing deep learning based algorithms for this task can be challenging due to the small pixel coverage of the anomaly and lack of suitable data since images with anomalies are rarely available in real-world scenarios [5]. Existing SOTA methods tackle this challenge using autoencoders [15, 47] and GAN based approaches [3, 43, 59], which use a thresholded pixel-wise difference between the input and reconstructed image to localize anomalies. But, their methods need to determine class-specific thresholds using anomalous training images which can be unavailable in real-world scenarios.

To tackle these drawbacks of using anomalous training images, we propose Convolutional Adversarial Variational autoencoder with Guided Attention (CAVGA), an unsupervised anomaly localization method which requires no anomalous training images. CAVGA comprises of a *convolutional latent variable* to preserve the spatial relation between the input and latent variable. Since real-world applications may have access to only limited training data [5], we propose to localize the anomalies by using supervision on attention maps. This

is motivated by the finding in [28] that attention based supervision can alleviate the need of using large amount of training data. Intuitively, without any prior knowledge of the anomaly, humans need to look at the entire image to identify the anomalous regions. Based on this idea, we propose an *attention expansion loss* where we encourage the network to generate an attention map that focuses on all normal regions of the image.

Since annotating segmentation training data can be laborious [22], in the case when the annotator provides few anomalous training images without ground truth segmented anomalous regions, we extend CAVGA to a weakly supervised setting. Here, we introduce a classifier in CAVGA and propose a *complementary guided attention loss* computed only for the normal images correctly predicted by the classifier. Using this complementary guided attention loss, we expand the normal attention but suppress the anomalous attention on the normal image, where normal/anomalous attention represents the areas affecting the classifier's normal/anomalous prediction identified by existing network visualization methods (e.g. Grad-CAM [49]). Fig. 1 (i) (a) illustrates our attention mechanism during training, and Fig. 1 (i) (b) demonstrates that the resulting normal attention and anomalous attention on the anomalous testing images are visually complementary, which is consistent with our intuition. Furthermore, Fig. 1 (ii) summarizes CAVGA's ability to outperform SOTA methods in anomaly localization on industrial inspection (MVTAD) [5], surveillance (mSTC) [31] and medical imaging (LAG) [29] datasets. We also show CAVGA's ability to outperform SOTA methods in anomaly detection on common benchmarks.

To the best of our knowledge, we are the first in anomaly localization to propose an end-to-end trainable framework with attention guidance which explicitly enforces the network to learn representations from the entire normal image. As compared to the prior works, our proposed approach CAVGA needs no anomalous training images to determine a class-specific threshold to localize the anomaly. Our contributions are:

- **An attention expansion loss (L_{ae})**, where we encourage the network to focus on the entire normal images in the unsupervised setting.
- **A complementary guided attention loss (L_{cga})**, which we use to minimize the anomalous attention and simultaneously expand the normal attention for the normal images correctly predicted by the classifier.
- **New SOTA**: In anomaly localization, CAVGA outperforms SOTA methods on the MVTAD and mSTC datasets in IoU and mean Area under ROC curve (AuROC) and also outperforms SOTA anomaly localization methods on LAG dataset in IoU. We also show CAVGA's ability to outperform SOTA methods for anomaly detection on the MVTAD, mSTC, LAG, MNIST [27], CIFAR-10 [25] and Fashion-MNIST [57] datasets in classification accuracy.

2   Related Works

Often used interchangeably, the terms anomaly localization and anomaly segmentation involve pixel-accurate segmentation of anomalous regions within an

Table 1: Comparison between CAVGA and other anomaly localization methods in the unsupervised setting in terms of the working properties. Among all the listed methods, only CAVGA satisfies all the listed properties

Does the method satisfy each property?	[3, 48] [6, 43]	[4]	[47]	[54] [50]	[13, 32] [2]	CAVGA
not using anomalous training images	N	N	Y	Y	Y	Y
localize **multiple** modes of anomalies	Y	N	N	N	Y	Y
pixel (not patch) based localization	Y	Y	N	Y	Y	Y
use **convolutional latent variable**	N	Y	N	N	N	Y

image [5]. They have been applied to industrial inspection settings to segment defective product parts [5], medical imaging to segment glaucoma in retina images [29], etc. Image based anomaly localization has not been fully studied as compared to anomaly detection, where methods such as [3, 4, 6, 43, 48] employ a thresholded pixel wise difference between the input and reconstructed image to segment the anomalous regions. [47] proposes an inpainter-detector network for patch-based localization in images. [13] proposes gradient descent on a regularized autoencoder while Liu *et al.* [32] (denoted as ADVAE) generate gradient based attention maps from the latent space of the trained model. We compare CAVGA with the existing methods relevant to anomaly localization in the unsupervised setting in Table 1 and show that among the listed methods, only CAVGA shows all the listed properties.

Anomaly detection involves determining an image as normal or anomalous [3]. One-class classification and anomaly detection are related to novelty detection [41] which has been widely studied in computer vision [3, 20, 35, 37, 53] and applied to video analysis [10], remote sensing [36], etc. With the advance in GANs [17], SOTA methods perform anomaly detection by generating realistic normal images during training [21, 22, 42, 46, 48]. [12] proposes to search the latent space of the generator for detecting anomalies. [41] introduces latent-space-sampling-based network with information-negative mining while [30] proposes normality score function based on capsule network's activation and reconstruction error. [2] proposes a deep autoencoder that learns the distribution of latent representation through autoregressive procedure. Unlike [7, 11, 44, 55] where anomalous training images are used for anomaly detection, CAVGA does not need anomalous training images.

3   Proposed Approach: CAVGA

3.1   Unsupervised Approach: CAVGA$_u$

Fig. 2 (a) illustrates CAVGA in the unsupervised setting (denoted as CAVGA$_u$). CAVGA$_u$ comprises of a convolutional latent variable to preserve the spatial information between the input and latent variable. Since attention maps obtained from feature maps illustrate the regions of the image responsible for specific
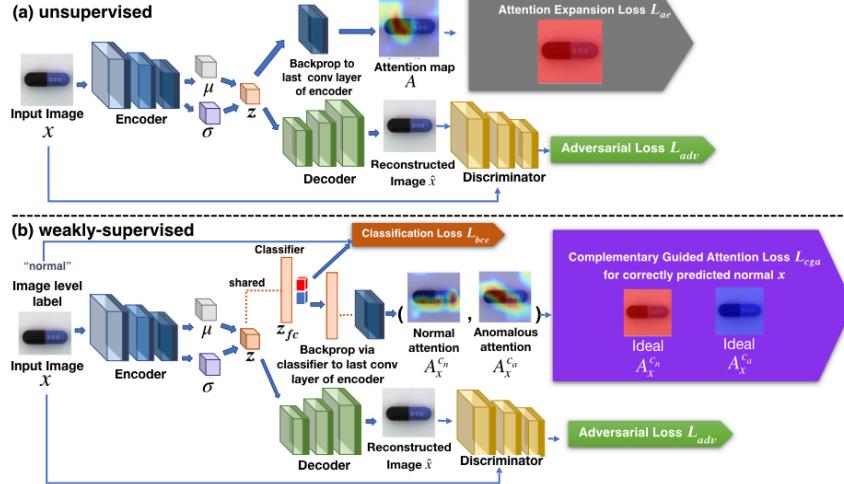
Fig. 2: (a) The framework of $CAVGA_u$ where the attention expansion loss L_{ae} guides the attention map A computed from the latent variable z to cover the entire normal image. (b) Illustration of $CAVGA_w$ with the complementary guided attention loss L_{cga} to minimize the anomalous attention $A_x^{c_a}$ and expand the normal attention $A_x^{c_n}$ for the normal images correctly predicted by the classifier

activation of neurons in the feature maps [58], we propose an attention expansion loss such that the feature representation of the latent variable encodes all the normal regions. This loss encourages the attention map generated from the latent variable to cover the entire normal training image as illustrated in Fig. 1 (i) (a). During testing, we localize the anomaly from the areas of the image that the attention map does not focus on.

Convolutional latent variable Variational Autoencoder (VAE) [23] is a generative model widely used for anomaly detection [24, 40]. The loss function of training a vanilla VAE can be formulated as:

$$L = L_R(x, \hat{x}) + KL(q_\phi(z|x)||p_\theta(z|x)), \tag{1}$$

where $L_R(x, \hat{x}) = \frac{-1}{N}\sum_{i=1}^N x_i log(\hat{x}_i) + (1-x_i)log(1-\hat{x}_i)$ is the reconstruction loss between the input (x) and reconstructed images $(\hat{x})$, and N is the total number of images. The posterior $p_\theta(z|x)$ is modeled using a standard Gaussian distribution prior $p(z)$ with the help of Kullback-Liebler (KL) divergence through $q_\phi(z|x)$. Since the vanilla VAE results in blurry reconstruction [26], we use a discriminator $(D(.))$ to improve the stability of the training and generate sharper reconstructed images $\hat{x}$ using adversarial learning [34] formulated as follows:

$$L_{adv} = -\frac{1}{N}\sum_{i=1}^N log(D(x_i)) + log(1 - D(\hat{x}_i)) \tag{2}$$

Unlike traditional autoencoders [6, 18] where the latent variable is flattened, inspired from [4], we use a convolutional latent variable to preserve the spatial relation between the input and the latent variable.

Attention expansion loss L_{ae} The main contribution of our work involves using supervision on attention maps to spatially localize the anomaly in the image. Most methods [3, 48, 53] employ a thresholded pixel-wise difference between the reconstructed image and the input image to localize the anomaly where the threshold is determined by using anomalous training images. However, CAVGA$_u$ learns to localize the anomaly using an attention map reflected through an end-to-end training process without the need of any anomalous training images. We use the feature representation of the latent variable z to compute the attention map (A). A is computed using Grad-CAM [49] such that $A_{i,j} \in [0, 1]$, where $A_{i,j}$ is the (i, j) element of A.

Intuitively, A obtained from feature maps focuses on the regions of the image based on the activation of neurons in the feature maps and its respective importance [58, 60]. Due to the lack of prior knowledge about the anomaly, in general, humans need to look at the entire image to identify anomalous regions. We use this notion to learn the feature representation of the entire normal image by proposing an attention expansion loss, where we encourage the network to generate an attention map covering all the normal regions. This attention expansion loss for each image $L_{ae,1}$ is defined as:

$$L_{ae,1} = \frac{1}{|A|} \sum_{i,j} (1 - A_{i,j}) \tag{3}$$

where $|A|$ is the total number of elements in A. The final attention expansion loss L_{ae} is the average of $L_{ae,1}$ over the N images. Since the idea of attention mechanisms involves locating the most salient regions in the image [29] which typically does not cover the entire image, we use L_{ae} as an additional supervision on the network, such that the trained network generates an attention map that covers all the normal regions. Fig. 1 (i) (a) shows that before using L_{ae} i.e. training CAVGA$_u$ only with adversarial learning ($L_{adv} + L$) does not encode all the normal regions into the latent variable, and that the attention map fails to cover the entire image, which is overcome after using L_{ae}. Furthermore, supervising on attention maps prevents the trained model to make inference based on incorrect areas and also alleviates the need of using large amount of training data as shown in [28], which is not explicitly enforced in existing methods [3, 6, 47].

We form the final objective function L_{final} below:

$$L_{final} = w_r L + w_{adv} L_{adv} + w_{ae} L_{ae}, \tag{4}$$

where w_r, w_{adv}, and w_{ae} are empirically set as $1, 1$, and 0.01 respectively.

During testing, we feed an image x_{test} into the encoder followed by the decoder, which reconstructs an image $\hat{x}_{test}$. As defined in [48], we compute the pixel-wise difference between $\hat{x}_{test}$ and x_{test} as the anomalous score s_a. Intuitively, if x_{test} is drawn from the learnt distribution of z, then s_a is small. Without

using any anomalous training images in the unsupervised setting, we normalize s_a between $[0, 1]$ and empirically set 0.5 as the threshold to detect an image as anomalous. The attention map A_{test} is computed from z using Grad-CAM and is inverted ($\mathbf{1}$ - A_{test}) to obtain an anomalous attention map which localizes the anomaly. Here, $\mathbf{1}$ refers to a matrix of all ones with the same dimensions as A_{test}. We empirically choose 0.5 as the threshold on the anomalous attention map to evaluate the localization performance.

3.2   Weakly Supervised Approach: CAVGA$_w$

CAVGA$_u$ can be further extended to a weakly supervised setting (denoted as CAVGA$_w$) where we explore the possibility of using few anomalous training images to improve the performance of anomaly localization. Given the labels of the anomalous and normal images without the pixel-wise annotation of the anomaly during training, we modify CAVGA$_u$ by introducing a binary classifier C at the output of z as shown in Fig. 2 (b) and train C using the binary cross entropy loss L_{bce}. Given an image x and its ground truth label y, we define $p \in \{c_a, c_n\}$ as the prediction of C, where c_a and c_n are anomalous and normal classes respectively. From Fig. 2 (b) we clone z into a new tensor, flatten it to form a fully connected layer z_{fc}, and add a 2-node output layer to form C. z and z_{fc} share parameters. Flattening z_{fc} enables a higher magnitude of gradient backpropagation from p [49].

Complementary guided attention loss L_{cga} Although, attention maps generated from a trained classifier have been used in weakly supervised semantic segmentation tasks [39, 49], to the best of our knowledge, we are the first to propose supervision on attention maps for anomaly localization in the weakly supervised setting. Since the attention map depends on the performance of C [28], we propose the complementary guided attention loss L_{cga} based on C's prediction to improve anomaly localization. We use Grad-CAM to compute the attention map for the anomalous class $A_x^{c_a}$ and the attention map for the normal class $A_x^{c_n}$ on the normal image x ($y = c_n$). Using $A_x^{c_a}$ and $A_x^{c_n}$, we propose L_{cga} where we minimize the areas covered by $A_x^{c_a}$ but simultaneously enforce $A_x^{c_n}$ to cover the entire normal image. Since the attention map is computed by backpropagating the gradients from p, any incorrect p would generate an undesired attention map. This would lead to the network learning to focus on erroneous areas of the image during training, which we avoid using L_{cga}. We compute L_{cga} only for the normal images correctly classified by the classifier i.e. if $p = y = c_n$. We define $L_{cga,1}$, the complementary guided attention loss for each image, in the weakly supervised setting as:

$$L_{cga,1} = \frac{\mathbb{1}\,(p = y = c_n)}{|A_x^{c_n}|} \sum_{i,j}(1 - (A_x^{c_n})_{i,j} + (A_x^{c_a})_{i,j}), \qquad (5)$$

where $\mathbb{1}\,(\cdot)$ is an indicator function. L_{cga} is the average of $L_{cga,1}$ over the N images. Our final objective function L_{final} is defined as:

$$L_{final} = w_r L + w_{adv}L_{adv} + w_c L_{bce} + w_{cga}L_{cga}, \qquad (6)$$

Table 2: Our experimental settings. Notations: u: unsupervised; w: weakly supervised; D_M: MNIST [27]; D_F: Fashion-MNIST [57]; D_C: CIFAR-10 [25]

property \ dataset	MVTAD [5]		mSTC [31]		LAG [29]	D_M	D_F	D_C
setting	u	w	u	w	u	u	u	u
# total classes	15	15	13	13	1	10	10	10
# normal training images	3629	3629	244875	244875	2632	~6k	6k	5k
# anomalous training images	0	35	0	1763	0	0	0	0
# normal testing images	467	467	21147	21147	800	~1k	1k	1k
# anomalous testing images	1223	1223	86404	86404	2392	~9k	9k	9k

where w_r, w_{adv}, w_c, and w_{cga} are empirically set as $1, 1, 0.001$, and 0.01 respectively. During testing, we use C to predict the input image x_{test} as anomalous or normal. The anomalous attention map A_{test} of x_{test} is computed when $y = c_a$. We use the same evaluation method as that in Sec. 3.1 for anomaly localization.

4   Experimental Setup

Benchmark datasets: We evaluate CAVGA on the MVTAD [5], mSTC [31] and LAG [29] datasets for anomaly localization, and the MVTAD, mSTC, LAG, MNIST [27], CIFAR-10 [25] and Fashion-MNIST [57] datasets for anomaly detection. Since STC dataset [31] is designed for video instead of image anomaly detection, we extract every 5th frame of the video from each scene for training and testing without using any temporal information. We term the modified STC dataset as mSTC and summarize the experimental settings in Table 2.

   Baseline methods: For anomaly localization, we compare CAVGA with AVID [47], AE_{L2} [6], AE_{SSIM} [6], AnoGAN [48], CNN feature dictionary (CN-NFD) [37], texture inspection (TI) [8], γ-VAE grad [13] (denoted as γ-VAE_g), LSA [2], ADVAE [32] and variation model (VM) [52] based approaches on the MVTAD and mSTC datasets. Since [13] does not provide the code for their method, we adapt the code from [1] and report its best result using our experimental settings. We also compare $CAVGA_u$ with CAM [60], GBP [51], Smooth-Grad [50] and Patho-GAN [54] on the LAG dataset. In addition, we compare $CAVGA_u$ with LSA [2], OCGAN [41], ULSLM [56], CapsNet PP-based and CapsNet RE-based [30] (denoted as $CapsNet_{PP}$ and $CapsNet_{RE}$), AnoGAN [48], ADGAN [12], and β-VAE [21] on the MNIST, CIFAR-10 and Fashion-MNIST datasets for anomaly detection.

   Architecture details: Based on the framework in Fig. 2 (a), we use the convolution layers of ResNet-18 [19] as our encoder pretrained from ImageNet [45] and finetuned on each category / scene individually. Inspired from [9], we propose to use the residual generator as our residual decoder by modifying it with a convolution layer interleaved between two upsampling layers. The skip connection added from the output of the upsampling layer to the output of the convolution layer, increases mutual information between observations and latent variable and also avoids latent variable collapse [14]. We use the discriminator of DC-GAN

Table 3: Performance comparison of anomaly localization in category-specific IoU, mean IoU ($\overline{\text{IoU}}$), and mean AuROC ($\overline{\text{AuROC}}$) on the MVTAD dataset. The darker cell color indicates better performance ranking in each row

Category	AVID [47]	AE_{SSIM} [6]	AE_{L2} [6]	AnoGAN [48]	$\gamma\text{-VAE}_g$ [13]	LSA [2]	ADVAE [32]	CAVGA -D_u	CAVGA -R_u	CAVGA -D_w	CAVGA -R_w
Bottle	0.28	0.15	0.22	0.05	0.27	0.27	0.27	0.30	0.34	0.36	0.39
Hazelnut	0.54	0.00	0.41	0.02	0.63	0.41	0.44	0.44	0.51	0.58	0.79
Capsule	0.21	0.09	0.11	0.04	0.24	0.22	0.11	0.25	0.31	0.38	0.41
Metal Nut	0.05	0.01	0.26	0.00	0.22	0.38	0.49	0.39	0.45	0.46	0.46
Leather	0.32	0.34	0.67	0.34	0.41	0.77	0.24	0.76	0.79	0.80	0.84
Pill	0.11	0.07	0.25	0.17	0.48	0.18	0.18	0.34	0.40	0.44	0.53
Wood	0.14	0.36	0.29	0.14	0.45	0.41	0.14	0.56	0.59	0.61	0.66
Carpet	0.25	0.69	0.38	0.34	0.79	0.76	0.10	0.71	0.73	0.70	0.81
Tile	0.09	0.04	0.23	0.08	0.38	0.32	0.23	0.31	0.38	0.47	0.81
Grid	0.51	0.88	0.83	0.04	0.36	0.20	0.02	0.32	0.38	0.42	0.55
Cable	0.27	0.01	0.05	0.01	0.26	0.36	0.18	0.37	0.44	0.49	0.51
Transistor	0.18	0.01	0.22	0.08	0.44	0.21	0.30	0.30	0.35	0.38	0.45
Toothbrush	0.43	0.08	0.51	0.07	0.37	0.48	0.14	0.54	0.57	0.60	0.63
Screw	0.22	0.03	0.34	0.01	0.38	0.38	0.17	0.42	0.48	0.51	0.66
Zipper	0.25	0.10	0.13	0.01	0.17	0.14	0.06	0.20	0.26	0.29	0.31
$\overline{\text{IoU}}$	0.26	0.19	0.33	0.09	0.39	0.37	0.20	0.41	0.47	0.50	0.59
$\overline{\text{AuROC}}$	0.78	0.87	0.82	0.74	0.86	0.79	0.86	0.85	0.89	0.92	0.93

[42] pretrained on the Celeb-A dataset [33] and finetuned on our data as our discriminator and term this network as CAVGA-R. For fair comparisons with the baseline approaches in terms of network architecture, we use the discriminator and generator of DC-GAN pretrained on the Celeb-A dataset as our encoder and decoder respectively. We keep the same discriminator as discussed previously and term this network as CAVGA-D. CAVGA-D_u and CAVGA-R_u are termed as CAVGA$_u$ in the unsupervised setting, and CAVGA-D_w and CAVGA-R_w as CAVGA$_w$ in weakly supervised setting respectively.

Training and evaluation: For anomaly localization and detection on the MVTAD, mSTC and LAG datasets, the network is trained only on normal images in the unsupervised setting. In the weakly supervised setting, since none of the baseline methods provide the number of anomalous training images they use to compute the threshold, we randomly choose 2% of the anomalous images along with all the normal training images for training. On the MNIST, CIFAR-10 and Fashion-MNIST datasets, we follow the same procedure as defined in [12] (training/testing uses single class as normal and the rest of the classes as anomalous. We train CAVGA-D_u using this normal class). For anomaly localization, we show the AuROC [5] and the Intersection-over-Union (IoU) between the generated attention map and the ground truth. Following [5], we use the mean of accuracy of correctly classified anomalous images and normal images to evaluate the performance of anomaly detection on both the normal and anomalous images on the MVTAD, mSTC and LAG datasets. On the MNIST, CIFAR-10, and Fashion-MNIST datasets, same as [12], we use AuROC for evaluation.

5   Experimental Results

We use the cell color in the quantitative result tables to denote the performance ranking in that row, where darker cell color means better performance.

Performance on anomaly localization: Fig. 3 (a) shows the qualitative results and Table 3 shows that $CAVGA_u$ localizes the anomaly better compared to the baselines on the MVTAD dataset. $CAVGA\text{-}D_u$ outperforms the best performing baseline method ($\gamma\text{-VAE}_g$) in mean IoU by 5%. Most baselines use anomalous training images to compute class-specific threshold to localize anomalies. *Needing no anomalous training images,* $CAVGA\text{-}D_u$ still outperforms all the mentioned baselines in mean IoU. In terms of mean AuROC, $CAVGA\text{-}D_u$ outperforms CNNFD, TI and VM by 9%, 12% and 10% respectively and achieves comparable results with best baseline method. Table 3 also shows that $CAVGA\text{-}D_w$ outperforms $CAVGA\text{-}D_u$ by 22% and 8% on mean IoU and mean AuROC respectively. $CAVGA\text{-}D_w$ also outperforms the baselines in mean AuROC. Fig. 4 illustrates that one challenge in anomaly localization is the low contrast between the anomalous regions and their background. In such scenarios, although still outperforming the baselines, CAVGA does not localize the anomaly well.
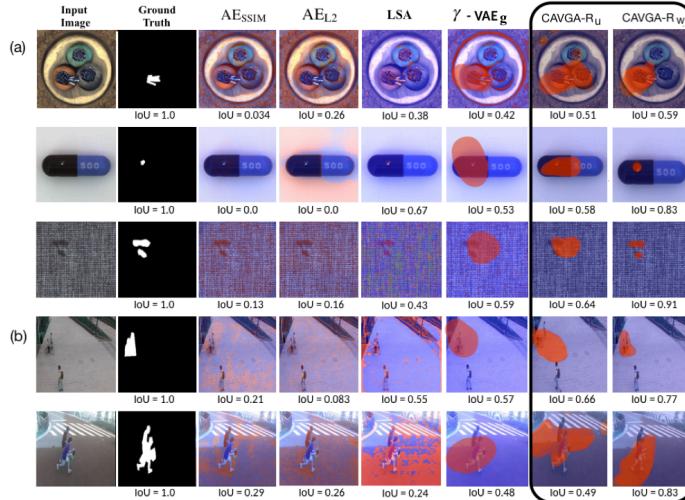

Fig. 3: Qualitative results on (a) MVTAD & (b) mSTC datasets respectively. The anomalous attention map (in red) depicts the localization of the anomaly

Fig. 3 (b) illustrates the qualitative results and Table 4 shows that CAVGA also outperforms the baseline methods in mean IoU and mean AuROC on the mSTC dataset. Table 5 shows that CAVGA outperforms the most competitive baseline Patho-GAN [54] by 16% in IoU on the LAG dataset. CAVGA is practically reasonable to train on a single GTX 1080Ti GPU, having comparable training and testing time with baseline methods.

Table 4: Performance comparison of anomaly localization in IoU and its mean ($\overline{\text{IoU}}$) along with anomaly detection in terms of mean of accuracy of correctly classified anomalous images and normal images on the mSTC dataset for each scene ID s_i. For anomaly localization, we also list the mean AuROC ($\overline{\text{AuROC}}$)

Task \ Method	s_i	γ-VAE$_g$ [13]	AVID [47]	LSA [2]	AE$_{SSIM}$ [6]	AE$_{L2}$ [6]	CAVGA -D$_u$	CAVGA -R$_u$	CAVGA -D$_w$	CAVGA -R$_w$
Localization	01	0.239	0.182	0.244	0.201	0.163	0.267	0.316	0.383	0.441
	02	0.206	0.206	0.183	0.081	0.172	0.190	0.234	0.257	0.349
	03	0.272	0.162	0.265	0.218	0.240	0.277	0.293	0.313	0.465
	04	0.290	0.263	0.271	0.118	0.125	0.283	0.349	0.360	0.381
	05	0.318	0.234	0.287	0.162	0.129	0.291	0.312	0.408	0.478
	06	0.337	0.314	0.238	0.215	0.198	0.344	0.420	0.455	0.589
	07	0.168	0.214	0.137	0.191	0.165	0.198	0.241	0.284	0.366
	08	0.220	0.168	0.233	0.069	0.056	0.219	0.254	0.295	0.371
	09	0.174	0.193	0.187	0.038	0.021	0.247	0.284	0.313	0.365
	10	0.146	0.137	0.146	0.116	0.141	0.149	0.166	0.245	0.295
	11	0.277	0.264	0.286	0.101	0.075	0.309	0.372	0.441	0.588
	12	0.162	0.180	0.108	0.203	0.164	0.098	0.141	0.207	0.263
$\overline{\text{IoU}}$		0.234	0.210	0.215	0.143	0.137	0.239	0.281	0.330	0.412
$\overline{\text{AuROC}}$		0.82	0.77	0.81	0.76	0.74	0.83	0.85	0.89	0.90
Detection	01	0.75	0.68	0.75	0.65	0.72	0.77	0.85	0.84	0.87
	02	0.75	0.75	0.79	0.70	0.61	0.76	0.84	0.89	0.90
	03	0.81	0.68	0.63	0.79	0.71	0.82	0.84	0.86	0.88
	04	0.83	0.71	0.79	0.81	0.66	0.80	0.80	0.81	0.83
	05	0.86	0.59	0.68	0.71	0.67	0.81	0.86	0.90	0.94
	06	0.59	0.62	0.58	0.47	0.55	0.64	0.67	0.65	0.70
	07	0.59	0.63	0.63	0.36	0.59	0.60	0.64	0.75	0.77
	08	0.77	0.73	0.75	0.69	0.70	0.74	0.74	0.76	0.80
	09	0.89	0.88	0.79	0.84	0.73	0.87	0.88	0.90	0.91
	10	0.64	0.80	0.84	0.83	0.88	0.88	0.92	0.94	0.94
	11	0.78	0.68	0.71	0.71	0.75	0.79	0.81	0.83	0.83
	12	0.71	0.66	0.63	0.65	0.52	0.76	0.79	0.81	0.83
avg		0.75	0.70	0.71	0.68	0.67	0.77	0.80	0.83	0.85

Table 5: Performance comparison of anomaly localization in IoU along with anomaly detection in terms of classification accuracy on the LAG dataset [29]

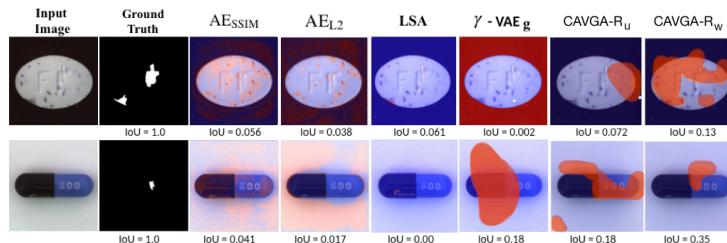| Task \ Method	CAM [60]	GBP [51]	SmoothGrad [50]	Patho-GAN [54]	CAVGA-D$_u$
Localization	0.13	0.09	0.14	0.37	0.43
Detection	0.68	0.84	0.79	0.89	0.90

Fig. 4: Examples of incorrect localization of the anomaly on the MVTAD dataset by CAVGA-R$_u$ and CAVGA-R$_w$

Table 6: The mean of accuracy of correctly classified anomalous images and normal images in anomaly detection on the MVTAD dataset

Category	AVID [47]	AE_{SSIM} [6]	AE_{L2} [6]	AnoGAN [48]	$\gamma\text{-VAE}_g$ [13]	LSA [2]	CAVGA $-D_u$	CAVGA $-R_u$	CAVGA $-D_w$	CAVGA $-R_w$
Bottle	0.88	0.88	0.80	0.69	0.86	0.86	0.89	0.91	0.93	0.96
Hazelnut	0.86	0.54	0.88	0.50	0.74	0.80	0.84	0.87	0.90	0.92
Capsule	0.85	0.61	0.62	0.58	0.86	0.71	0.83	0.87	0.89	0.93
Metal Nut	0.63	0.54	0.73	0.50	0.78	0.67	0.67	0.71	0.81	0.88
Leather	0.58	0.46	0.44	0.52	0.71	0.70	0.71	0.75	0.80	0.84
Pill	0.86	0.60	0.62	0.62	0.80	0.85	0.88	0.91	0.93	0.97
Wood	0.83	0.83	0.74	0.68	0.89	0.75	0.85	0.88	0.89	0.89
Carpet	0.70	0.67	0.50	0.49	0.67	0.74	0.73	0.78	0.80	0.82
Tile	0.66	0.52	0.77	0.51	0.81	0.70	0.70	0.72	0.81	0.86
Grid	0.59	0.69	0.78	0.51	0.83	0.54	0.75	0.78	0.79	0.81
Cable	0.64	0.61	0.56	0.53	0.56	0.61	0.63	0.67	0.86	0.97
Transistor	0.58	0.52	0.71	0.67	0.70	0.50	0.73	0.75	0.80	0.89
Toothbrush	0.73	0.74	0.98	0.57	0.89	0.89	0.91	0.97	0.96	0.99
Screw	0.66	0.51	0.69	0.35	0.71	0.75	0.77	0.78	0.79	0.79
Zipper	0.84	0.80	0.80	0.59	0.67	0.88	0.87	0.94	0.95	0.96
mean	0.73	0.63	0.71	0.55	0.77	0.73	0.78	0.82	0.86	0.90

Performance on anomaly detection: Table 6 shows that $CAVGA_u$ outperforms the baselines in the mean of accuracy of correctly classified anomalous images and normal images on the MVTAD dataset. CAVGA-D_u outperforms the best performing baseline (γ-VAE$_g$) in mean of classification accuracy by 1.3%. Table 4 and Table 5 show that CAVGA outperforms the baseline methods in classification accuracy on both the mSTC and LAG datasets by 2.6% and 1.1% respectively. Furthermore, Table 7 shows that CAVGA-D_u outperforms all the baselines in mean AuROC in the unsupervised setting on the MNIST, CIFAR-10 and Fashion-MNIST datasets. CAVGA-D_u also outperforms MemAE [16] and β-VAE [21] by 1.1% and 8% on MNIST and by 21% and 38% on CIFAR-10 datasets respectively. CAVGA-D_u also outperforms all the listed baselines in mean AuROC on the Fashion-MNIST dataset.

6 Ablation Study

All the ablation studies are performed on 15 categories on the MVTAD dataset, of which 5 are reported here. The mean of all 15 categories is shown in Table 8. We illustrate the effectiveness of the convolutional z in CAVGA, L_{ae} in the unsupervised setting, and L_{cga} in the weakly supervised setting. The qualitative results are shown in Fig. 5. The column IDs to refer to the columns in Table 8.

Effect of convolutional latent variable z: To show the effectiveness of the convolutional z, we flatten the output of the encoder of CAVGA-R_u and CAVGA-R_w, and connect it to a fully connected layer as latent variable. Following [6], the dimension of latent variable is chosen as 100. We call these network as CAVGA-R_u^* and CAVGA-R_w^* in the unsupervised and weakly supervised settings respectively. In the unsupervised setting, we train CAVGA-R_u and CAVGA-R_u^* using $L + L_{adv}$ as our objective function and compute the anomalous attention

Table 7: Performance comparison of anomaly detection in terms of AuROC and mean AuROC with the SOTA methods on MNIST (D_M) and CIFAR-10 (D_C) datasets . We also report the mean AuROC on Fashion-MNIST (D_F) dataset

Dataset	Class	γ-VAE$_g$ [13]	LSA [2]	OCGAN [41]	ULSLM [56]	CapsNet$_{PP}$ [30]	CapsNet$_{RE}$ [30]	AnoGAN [48]	ADGAN [12]	CAVGA -D$_u$
D_M [27]	0	0.991	0.993	0.998	0.991	0.998	0.947	0.990	0.999	0.994
	1	0.996	0.999	0.999	0.972	0.990	0.907	0.998	0.992	0.997
	2	0.983	0.959	0.942	0.919	0.984	0.970	0.888	0.968	0.989
	3	0.978	0.966	0.963	0.943	0.976	0.949	0.913	0.953	0.983
	4	0.976	0.956	0.975	0.942	0.935	0.872	0.944	0.960	0.977
	5	0.972	0.964	0.980	0.872	0.970	0.966	0.912	0.955	0.968
	6	0.993	0.994	0.991	0.988	0.942	0.909	0.925	0.980	0.988
	7	0.981	0.980	0.981	0.939	0.987	0.934	0.964	0.950	0.986
	8	0.980	0.953	0.939	0.960	0.993	0.929	0.883	0.959	0.988
	9	0.967	0.981	0.981	0.967	0.990	0.871	0.958	0.965	0.991
	mean	0.982	0.975	0.975	0.949	0.977	0.925	0.937	0.968	0.986
D_C [25]	0	0.702	0.735	0.757	0.740	0.622	0.371	0.610	0.661	0.653
	1	0.663	0.580	0.531	0.747	0.455	0.737	0.565	0.435	0.784
	2	0.680	0.690	0.640	0.628	0.671	0.421	0.648	0.636	0.761
	3	0.713	0.542	0.620	0.572	0.675	0.588	0.528	0.488	0.747
	4	0.770	0.761	0.723	0.678	0.683	0.388	0.670	0.794	0.775
	5	0.689	0.546	0.620	0.602	0.635	0.601	0.592	0.640	0.552
	6	0.805	0.751	0.723	0.753	0.727	0.491	0.625	0.685	0.813
	7	0.588	0.535	0.575	0.685	0.673	0.631	0.576	0.559	0.745
	8	0.813	0.717	0.820	0.781	0.710	0.410	0.723	0.798	0.801
	9	0.744	0.548	0.554	0.795	0.466	0.671	0.582	0.643	0.741
	mean	0.717	0.641	0.656	0.736	0.612	0.531	0.612	0.634	0.737
D_F [57]	mean	0.873	0.876	-	-	0.765	0.679	-	-	0.885

Table 8: The ablation study on 5 randomly chosen categories showing anomaly localization in IoU on the MVTAD dataset. The mean of all 15 categories is reported. CAVGA-R$_u^*$ and CAVGA-R$_w^*$ are our base architecture with a flattened z in the unsupervised and weakly supervised settings respectively. "conv z" means using convolutional z

Method	CAVGA -R$_u^*$	CAVGA -R$_u^*$ + L_{ae}	CAVGA -R$_u$ + conv z	CAVGA -R$_u$ + conv z + L_{ae}	CAVGA -R$_w^*$	CAVGA -R$_w^*$ + L_{cga}	CAVGA -R$_w$ + conv z	CAVGA -R$_w$ + conv z + L_{cga}
Category								
Column ID	c_1	c_2	c_3	c_4	c_5	c_6	c_7	c_8
Bottle	0.24	0.27	0.26	0.33	0.16	0.34	0.28	0.39
Hazelnut	0.16	0.26	0.31	0.47	0.51	0.76	0.67	0.79
Capsule	0.09	0.22	0.14	0.31	0.18	0.36	0.27	0.41
Metal Nut	0.28	0.38	0.34	0.45	0.25	0.38	0.28	0.46
Leather	0.55	0.71	0.64	0.79	0.72	0.79	0.75	0.84
mean	0.24	0.34	0.33	0.47	0.39	0.52	0.48	0.60

map from the feature map of the latent variable during inference. Similarly, in the weakly supervised setting, we train CAVGA-R$_w$ and CAVGA-R$_w^*$ using $L + L_{adv} + L_{bce}$ as our objective function and compute the anomalous attention map from the classifier's prediction during inference. Comparing column c_1 with
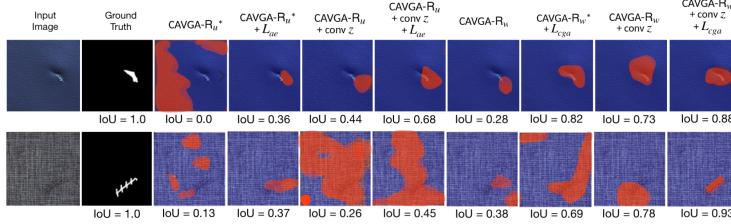
Fig. 5: Qualitative results of the ablation study to illustrate the performance of the anomaly localization on the MVTAD dataset

c_3 and c_5 with c_7 in Table 8, we observe that preserving the spatial relation of the input and latent variable through the convolutional z improves the IoU in anomaly localization without the use of L_{ae} in the unsupervised setting and L_{cga} in the weakly supervised setting. Furthermore, comparing column c_2 with c_4 and c_6 with c_8 in Table 8, we observe that using convolutional z in CAVGA-R$_u$ and CAVGA-R$_w$ outperforms using a flattened latent variable even with the help of L_{ae} in the unsupervised setting and L_{cga} in the weakly supervised setting.

Effect of attention expansion loss L_{ae}: To test the effectiveness of using L_{ae} in the unsupervised setting, we train CAVGA-R$_u^*$ and CAVGA-R$_u$ with eq. 4. During inference, the anomalous attention map is computed to localize the anomaly. Comparing column c_1 with c_2 and c_3 with c_4 in Table 8, we observe that L_{ae} enhances the IoU regardless of a flattened or convolutional latent variable.

Effect of complementary guided attention loss L_{cga}: We show the effectiveness of L_{cga} by training CAVGA-R$_w^*$ and CAVGA-R$_w$ using eq. 6. Comparing column c_5 with c_6 and c_7 with c_8 in Table 8, we find that using L_{cga} enhances the IoU regardless of a flattened or convolutional latent variable.

7   Conclusion

We propose an end-to-end convolutional adversarial variational autoencoder using guided attention which is a novel use of this technique for anomaly localization. Applicable to different network architectures, our attention expansion loss and complementary guided attention loss improve the performance of anomaly localization in the unsupervised and weakly supervised (with only 2% extra anomalous images for training) settings respectively. We quantitatively and qualitatively show that CAVGA outperforms the state-of-the-art (SOTA) anomaly localization methods on the MVTAD, mSTC and LAG datasets. We also show CAVGA's ability to outperform SOTA anomaly detection methods on the MV-TAD, mSTC, LAG, MNIST, Fashion-MNIST and CIFAR-10 datasets.

Bibliography

[1] Code for iterative energy-based projection on a normal data manifold for anomaly localization. `https://qiita.com/kogepan102/items/122b2862ad5a51180656`, accessed on: 2020-02-29

[2] Abati, D., Porrello, A., Calderara, S., Cucchiara, R.: Latent space autoregression for novelty detection. In: Proceedings of the IEEE Conference on Computer Vision and Pattern Recognition. pp. 481–490 (2019)

[3] Akcay, S., Atapour-Abarghouei, A., Breckon, T.P.: GANomaly: Semi-supervised anomaly detection via adversarial training. In: Asian Conference on Computer Vision. pp. 622–637. Springer (2018)

[4] Baur, C., Wiestler, B., Albarqouni, S., Navab, N.: Deep autoencoding models for unsupervised anomaly segmentation in brain mr images. In: International MICCAI Brainlesion Workshop. pp. 161–169. Springer (2018)

[5] Bergmann, P., Fauser, M., Sattlegger, D., Steger, C.: MVTec AD–a comprehensive real-world dataset for unsupervised anomaly detection. In: Proceedings of the IEEE Conference on Computer Vision and Pattern Recognition. pp. 9592–9600 (2019)

[6] Bergmann, P., Löwe, S., Fauser, M., Sattlegger, D., Steger, C.: Improving unsupervised defect segmentation by applying structural similarity to autoencoders. In: International Joint Conference on Computer Vision, Imaging and Computer Graphics Theory and Applications (VISIGRAPP). vol. 5 (2019)

[7] Bian, J., Hui, X., Sun, S., Zhao, X., Tan, M.: A novel and efficient cvae-gan-based approach with informative manifold for semi-supervised anomaly detection. IEEE Access **7**, 88903–88916 (2019)

[8] Böttger, T., Ulrich, M.: Real-time texture error detection on textured surfaces with compressed sensing. Pattern Recognition and Image Analysis **26**(1), 88–94 (2016)

[9] Brock, A., Donahue, J., Simonyan, K.: Large scale GAN training for high fidelity natural image synthesis. In: International Conference on Learning Representations (2019)

[10] Cheng, K.W., Chen, Y.T., Fang, W.H.: Abnormal crowd behavior detection and localization using maximum sub-sequence search. In: Proceedings of the 4th ACM/IEEE international workshop on Analysis and retrieval of tracked events and motion in imagery stream. pp. 49–58. ACM (2013)

[11] Daniel, T., Kurutach, T., Tamar, A.: Deep variational semi-supervised novelty detection. arXiv preprint arXiv:1911.04971 (2019)

[12] Deecke, L., Vandermeulen, R., Ruff, L., Mandt, S., Kloft, M.: Image anomaly detection with generative adversarial networks. In: Joint European Conference on Machine Learning and Knowledge Discovery in Databases. pp. 3–17. Springer (2018)

[13] Dehaene, D., Frigo, O., Combrexelle, S., Eline, P.: Iterative energy-based projection on a normal data manifold for anomaly localization. International Conference on Learning Representations (2020)

[14] Dieng, A.B., Kim, Y., Rush, A.M., Blei, D.M.: Avoiding latent variable collapse with generative skip models. In: The 22nd International Conference on Artificial Intelligence and Statistics. pp. 2397–2405 (2019)

[15] Dimokranitou, A.: Adversarial autoencoders for anomalous event detection in images. Ph.D. thesis (2017)

[16] Gong, D., Liu, L., Le, V., Saha, B., Mansour, M.R., Venkatesh, S., Hengel, A.v.d.: Memorizing normality to detect anomaly: Memory-augmented deep autoencoder for unsupervised anomaly detection. In: Proceedings of the IEEE International Conference on Computer Vision. pp. 1705–1714 (2019)

[17] Goodfellow, I., Pouget-Abadie, J., Mirza, M., Xu, B., Warde-Farley, D., Ozair, S., Courville, A., Bengio, Y.: Generative adversarial nets. In: Advances in neural information processing systems. pp. 2672–2680 (2014)

[18] Gutoski, M., Aquino, N.M.R., Ribeiro, M., Lazzaretti, E., Lopes, S.: Detection of video anomalies using convolutional autoencoders and one-class support vector machines. In: XIII Brazilian Congress on Computational Intelligence, 2017 (2017)

[19] He, K., Zhang, X., Ren, S., Sun, J.: Deep residual learning for image recognition. In: Proceedings of the IEEE Conference on Computer Vision and Pattern Recognition. pp. 770–778 (2016)

[20] Hendrycks, D., Mazeika, M., Dietterich, T.G.: Deep anomaly detection with outlier exposure. In: International Conference on Learning Representations (2019)

[21] Higgins, I., Matthey, L., Pal, A., Burgess, C., Glorot, X., Botvinick, M., Mohamed, S., Lerchner, A.: beta-VAE: Learning basic visual concepts with a constrained variational framework. International Conference on Learning Representations 2(5), 6 (2017)

[22] Kimura, D., Chaudhury, S., Narita, M., Munawar, A., Tachibana, R.: Adversarial discriminative attention for robust anomaly detection. In: The IEEE Winter Conference on Applications of Computer Vision (WACV) (March 2020)

[23] Kingma, D.P., Welling, M.: Auto-encoding variational bayes. In: International Conference on Learning Representations (2014)

[24] Kiran, B., Thomas, D., Parakkal, R.: An overview of deep learning based methods for unsupervised and semi-supervised anomaly detection in videos. Journal of Imaging 4(2), 36 (2018)

[25] Krizhevsky, A., Hinton, G., et al.: Learning multiple layers of features from tiny images. Tech. rep., Citeseer (2009)

[26] Larsen, A.B.L., Sønderby, S.K., Larochelle, H., Winther, O.: Autoencoding beyond pixels using a learned similarity metric. In: International Conference on Machine Learning (2016)

[27] LeCun, Y., Bottou, L., Bengio, Y., Haffner, P., et al.: Gradient-based learning applied to document recognition. Proceedings of the IEEE 86(11), 2278–2324 (1998)

[28] Li, K., Wu, Z., Peng, K.C., Ernst, J., Fu, Y.: Tell me where to look: Guided attention inference network. In: Proceedings of the IEEE Conference on Computer Vision and Pattern Recognition. pp. 9215–9223 (2018)

[29] Li, L., Xu, M., Wang, X., Jiang, L., Liu, H.: Attention based glaucoma detection: A large-scale database and cnn model. In: The IEEE Conference on Computer Vision and Pattern Recognition (CVPR) (June 2019)

[30] Li, X., Kiringa, I., Yeap, T., Zhu, X., Li, Y.: Exploring deep anomaly detection methods based on capsule net. International Conference on Machine Learning 2019 Workshop on Uncertainty and Robustness in Deep Learning (2019)

[31] Liu, W., Luo, W., Lian, D., Gao, S.: Future frame prediction for anomaly detection–a new baseline. In: Proceedings of the IEEE Conference on Computer Vision and Pattern Recognition. pp. 6536–6545 (2018)

[32] Liu, W., Li, R., Zheng, M., Karanam, S., Wu, Z., Bhanu, B., Radke, R.J., Camps, O.: Towards visually explaining variational autoencoders. Proceedings of the IEEE Conference on Computer Vision and Pattern Recognition (2020)

[33] Liu, Z., Luo, P., Wang, X., Tang, X.: Deep learning face attributes in the wild. In: Proceedings of International Conference on Computer Vision (ICCV) (December 2015)

[34] Makhzani, A., Shlens, J., Jaitly, N., Goodfellow, I., Frey, B.: Adversarial autoencoders. In: International Conference on Learning Representations (2016)

[35] Masana, M., Ruiz, I., Serrat, J., van de Weijer, J., Lopez, A.M.: Metric learning for novelty and anomaly detection. In: British Machine Vision Conference (BMVC) (2018)

[36] Matteoli, S., Diani, M., Theiler, J.: An overview of background modeling for detection of targets and anomalies in hyperspectral remotely sensed imagery. IEEE Journal of Selected Topics in Applied Earth Observations and Remote Sensing **7**(6), 2317–2336 (2014)

[37] Napoletano, P., Piccoli, F., Schettini, R.: Anomaly detection in nanofibrous materials by CNN-based self-similarity. Sensors **18**(1), 209 (2018)

[38] Nguyen, P., Liu, T., Prasad, G., Han, B.: Weakly supervised action localization by sparse temporal pooling network. In: Proceedings of the IEEE Conference on Computer Vision and Pattern Recognition. pp. 6752–6761 (2018)

[39] Oquab, M., Bottou, L., Laptev, I., Sivic, J.: Is object localization for free?-weakly-supervised learning with convolutional neural networks. In: Proceedings of the IEEE Conference on Computer Vision and Pattern Recognition. pp. 685–694 (2015)

[40] Pawlowski, N., Lee, M.C., Rajchl, M., McDonagh, S., Ferrante, E., Kamnitsas, K., Cooke, S., Stevenson, S., Khetani, A., Newman, T., et al.: Unsupervised lesion detection in brain CT using bayesian convolutional autoencoders. In: Medical Imaging with Deep Learning (2018)

[41] Perera, P., Nallapati, R., Xiang, B.: OCGAN: One-class novelty detection using GANs with constrained latent representations. In: Proceedings of the

IEEE Conference on Computer Vision and Pattern Recognition. pp. 2898–2906 (2019)

[42] Radford, A., Metz, L., Chintala, S.: Unsupervised representation learning with deep convolutional generative adversarial networks. In: International Conference on Learning Representations (2016)

[43] Ravanbakhsh, M., Sangineto, E., Nabi, M., Sebe, N.: Training adversarial discriminators for cross-channel abnormal event detection in crowds. In: 2019 IEEE Winter Conference on Applications of Computer Vision (WACV). pp. 1896–1904. IEEE (2019)

[44] Ruff, L., Vandermeulen, R.A., Görnitz, N., Binder, A., Müller, E., Müller, K.R., Kloft, M.: Deep semi-supervised anomaly detection. International Conference on Learning Representations (2020)

[45] Russakovsky, O., Deng, J., Su, H., Krause, J., Satheesh, S., Ma, S., Huang, Z., Karpathy, A., Khosla, A., Bernstein, M., et al.: ImageNet large scale visual recognition challenge. International journal of computer vision **115**(3), 211–252 (2015)

[46] Sabokrou, M., Khalooei, M., Fathy, M., Adeli, E.: Adversarially learned one-class classifier for novelty detection. In: Proceedings of the IEEE Conference on Computer Vision and Pattern Recognition. pp. 3379–3388 (2018)

[47] Sabokrou, M., Pourreza, M., Fayyaz, M., Entezari, R., Fathy, M., Gall, J., Adeli, E.: Avid: Adversarial visual irregularity detection. In: Asian Conference on Computer Vision. pp. 488–505. Springer (2018)

[48] Schlegl, T., Seeböck, P., Waldstein, S.M., Schmidt-Erfurth, U., Langs, G.: Unsupervised anomaly detection with generative adversarial networks to guide marker discovery. In: International Conference on Information Processing in Medical Imaging. pp. 146–157. Springer (2017)

[49] Selvaraju, R.R., Cogswell, M., Das, A., Vedantam, R., Parikh, D., Batra, D.: Grad-cam: Visual explanations from deep networks via gradient-based localization. In: Proceedings of the IEEE International Conference on Computer Vision. pp. 618–626 (2017)

[50] Smilkov, D., Thorat, N., Kim, B., Viégas, F., Wattenberg, M.: SmoothGrad: removing noise by adding noise. arXiv preprint arXiv:1706.03825 (2017)

[51] Springenberg, J.T., Dosovitskiy, A., Brox, T., Riedmiller, M.: Striving for simplicity: The all convolutional net. arXiv preprint arXiv:1412.6806 (2014)

[52] Steger, C.: Similarity measures for occlusion, clutter, and illumination invariant object recognition. In: Joint Pattern Recognition Symposium. pp. 148–154. Springer (2001)

[53] Vu, H.S., Ueta, D., Hashimoto, K., Maeno, K., Pranata, S., Shen, S.M.: Anomaly detection with adversarial dual autoencoders. arXiv preprint arXiv:1902.06924 (2019)

[54] Wang, X., Xu, M., Li, L., Wang, Z., Guan, Z.: Pathology-aware deep network visualization and its application in glaucoma image synthesis. In: International Conference on Medical Image Computing and Computer-Assisted Intervention. pp. 423–431. Springer (2019)

[55] Wang, Z., Fan, M., Muknahallipatna, S., Lan, C.: Inductive multi-view semi-supervised anomaly detection via probabilistic modeling. In: 2019 IEEE

International Conference on Big Knowledge (ICBK). pp. 257–264. IEEE (2019)

[56] Wolf, L., Benaim, S., Galanti, T.: Unsupervised learning of the set of local maxima. International Conference on Learning Representations (2019)

[57] Xiao, H., Rasul, K., Vollgraf, R.: Fashion-MNIST: a novel image dataset for benchmarking machine learning algorithms. arXiv preprint arXiv:1708.07747 (2017)

[58] Zagoruyko, S., Komodakis, N.: Paying more attention to attention: Improving the performance of convolutional neural networks via attention transfer. In: International Conference on Learning Representations (2017)

[59] Zenati, H., Foo, C.S., Lecouat, B., Manek, G., Chandrasekhar, V.R.: Efficient GAN-based anomaly detection. arXiv preprint arXiv:1802.06222 (2018)

[60] Zhou, B., Khosla, A., Lapedriza, A., Oliva, A., Torralba, A.: Learning deep features for discriminative localization. In: Proceedings of the IEEE conference on computer vision and pattern recognition. pp. 2921–2929 (2016)